



ELSEVIER

1 January 2000

OPTICS  
COMMUNICATIONS

Optics Communications 173 (2000) 315–321

www.elsevier.com/locate/optcom

# An inexpensive diode-pumped mode-locked Nd:YVO<sub>4</sub> laser for nonlinear optical microscopy

P.K. Yang, J.Y. Huang \*

*Institute of Electro-Optical Engineering, Chiao Tung University, Hsinchu, Taiwan*

Received 20 July 1999; received in revised form 15 September 1999; accepted 5 October 1999

## Abstract

We report an inexpensive diode-pumped Nd:YVO<sub>4</sub> laser mode-locked with combined effects of nonlinear mirror (NLM) and cascaded second-order optical nonlinearities (CSON) in a KTP crystal. Detailed analysis, which takes into account the transverse effect of cavity modes, shows that the CSON effect dominates the mode locking process. The resulting self-defocusing lens couples with an aperture appearing in the gain medium and then produces a cavity loss modulation. The mode locking self starts at a pump power of 2.2 W with a 35% transmission output coupler and generates pulses with a duration of 14 ps and an averaged power of 350 mW. The laser was shown to be useful for probing polar structures of nonlinear optical materials with second harmonic microscopy. © 2000 Elsevier Science B.V. All rights reserved.

PACS: 42.55.X; 42.60.F; 42.65

Keywords: Mode locking; Diode-pumped; Solid state laser; Second-harmonic microscopy

Continuous-wave mode-locked lasers are useful for nonlinear optical spectroscopy and microscopy. In the past several years, a variety of mode-locking schemes had been developed for generating ultra-short laser pulses. Among these developments, Kerr lens mode-locking [1,2] is the most notable method. However, this scheme usually yields fairly high mode-locking threshold and requires critical cavity alignment. More recently, an alternative method based on semiconductor saturable absorbers, such as Bragg reflector (SBR) [3] or antiresonant Fabry–

Perot saturable absorber (A-FPSA) [4], has received increasing attention for its lack of demand for critical cavity alignment and low mode-locking threshold. Unfortunately, this mode locking method requires fairly sophisticated material growth technique for preparing SBR and A-FPSA structures. In addition, the saturable absorption bandwidth of these semiconductor structures is limited.

Effects of nonlinear mirror (NLM) [5–7] and cascaded second-order nonlinearities (CSON) [8–13] with a nonlinear optical crystal produce stronger mode-locking strength than that from a single third-order process. It is therefore interesting to employ these effects in a diode-pumped laser to accomplish the goal of a compact design with low mode locking

\* Corresponding author. Fax: +886-3-571-6631; e-mail: jyhuang@cc.nctu.edu.tw

threshold. In this paper, such a laser that uses Nd:YVO<sub>4</sub> as the gain medium is reported.

The layout of our laser resonator is depicted in Fig. 1(a). A Nd:YVO<sub>4</sub> laser crystal with 1% doping and dimensions of 5 × 5 × 6 mm is used. A 4 W diode laser at 808 nm longitudinally pumps the laser crystal. One surface of the Nd:YVO<sub>4</sub> crystal is Brewster-cut and the other surface is coated to have high reflection at 1064 nm and high transmission at 808 nm. The nonlinear crystal used in our experiment is a 6 mm long KTP crystal cut to fulfil the type-II phase matching at  $\varphi = 23.5^\circ$  on the  $x$ - $y$  plane of the crystal. The cavity is folded at mirror M1 to compensate astigmatism on entering the Brewster angled surface of the laser crystal. The output coupler transmits 35% of the fundamental beam but has high reflection at 532 nm.

The plano-convex lens L2 in Fig. 1(a) produces a radial dependent phase mismatch between the fundamental and the second harmonic waves. The phase mismatch causes an incomplete back-conversion from the second harmonic to the fundamental beam, which leads to a cavity loss for the fundamental field. To estimate how much the backward conversion is blocked, we introduce a window function on L2

$$m(r, \varphi) = \cos^2 \left[ \frac{\pi}{l_c} \left( R - \sqrt{R^2 - r^2} \right) + \frac{\varphi}{2} \right], \quad (1)$$

where  $R$  is the radius of curvature of the convex surface,  $l_c = \pi/\Delta k_g$  denotes the coherent length of the lens material, and  $\varphi$  is a parameter that accounts for the phase dependence of on-axis back conversion. When  $\varphi$  is zero, the on-axis second harmonic beam can be fully back-converted to the fundamental wave during the second travel through the nonlinear crystal. In our setup,  $R = 23$  mm and  $l_c = 24$   $\mu\text{m}$  were chosen. The fundamental wave generated from back conversion, was then traced backward from the nonlinear crystal to L2. We approximate the resulting transverse intensity distribution on L2 with a Gaussian profile  $I(r) = [2/(\pi w_{\text{eff}}^2)] \exp[-2(r^2/w_{\text{eff}}^2)]$ . The effective beam waist can be estimated with  $1/w_{\text{eff}}^2 = 1/w_{2\omega}^2 - 1/w_\omega^2$ . By using  $w_{2\omega} = w_\omega/\sqrt{2}$ , we then have  $w_{\text{eff}} = w_\omega = 36$   $\mu\text{m}$ . The blocking ratio was calculated with  $\int_0^\infty I(r)[1 - m(r)]2\pi r dr$ . The integral has a minimal value of

0.03 at  $\varphi = -0.35$  rad. The blocking ratio for our setup is smaller than the transmission loss of the fundamental beam at the output coupler. Note that to successfully achieve mode locking with CSON, the roundtrip loss of the second harmonic beam from the nonlinear crystal to the output coupler should be smaller than that of the fundamental beam. If the condition were not met, pulse formation would cause additional cavity losses, which then counteracts with the mode-locking process.

It merits pointing out that the insertion of L2 benefits mode locking by reducing the aberration in nonlinear phase shift. The decrease in aberration can be better understood by expanding  $I(r)$  and  $m(r, \varphi)I(r)$  into power series of  $r$

$$\begin{aligned} \frac{\pi w^2}{2} I(r) &\cong 1 - \frac{2r^2}{w^2} + \frac{2r^4}{w^4} + O(r^6) \\ &= 1 - 15.76r^2 + 124.44r^4 + O(r^6), \end{aligned}$$

$$\begin{aligned} m(r, \varphi) \frac{\pi w^2}{2} I(r) &\cong \left( 1 - \frac{\varphi^2}{8} \right) - \left( \frac{2}{w^2} + \frac{\pi\varphi}{4Rl_c} \right) r^2 \\ &\quad - \left[ \frac{2}{w^4} \left( 1 - \frac{\varphi^2}{8} \right) - \frac{\pi^2}{8R^2l_c} \right. \\ &\quad \left. + \frac{\pi\varphi}{2Rl_c w^2} \right] r^4 + O(r^6) \quad (3) \\ &= 0.99 \times (1 - 15.51r^2 + 0.144r^4) + O(r^6). \end{aligned}$$

Here  $r$  is expressed in units of millimeters and  $\varphi = -0.35$  rad. Note that the coefficient of the fourth-order term in  $I(r, \varphi)$  is decreased significantly, indicating that deviation from quadratic dependence in the nonlinear phase shift can be effectively reduced by L2.

To achieve mode locking, we first oriented KTP at its type-II ( $e + o \rightarrow e$ ) phase-matching direction. The  $z$  axis of the crystal was rotated  $45^\circ$  from the polarization of the incident fundamental beam to

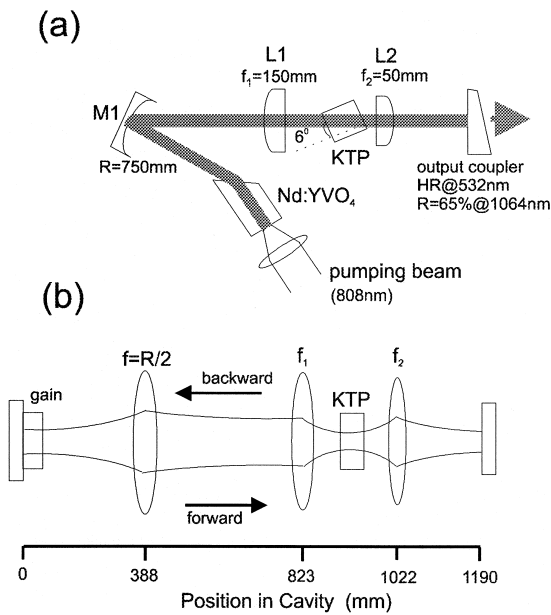


Fig. 1. (a) Schematic of the experimental setup; and (b) the corresponding effective cavity configuration.

have identical *e*- and *o*-ray components. We then detuned the crystal from its phase-matching direction to accommodate a spreading in *k*-space from a tightly focused Gaussian beam [14]. The angular detuning maximizes the second-harmonic conversion in the first trip. Mode locking can then be achieved by optimizing the back-conversion efficiency with a fine angular adjustment of the KTP crystal. The fine-tuning introduces a phase mismatch between the fundamental and the second harmonic waves before they re-enter into the nonlinear crystal. In our experiment, the laser can be mode locked with the surface normal of the KTP crystal tilting from the beam propagating direction by an external angle of  $6^\circ$ .

The CW mode-locking threshold pump power was found to be 2.2 W with an output coupler that has 35% transmission at  $1.064 \mu\text{m}$  and high reflection at 532 nm. At the pumping level of 2.5 W, we obtain a mode-locking output of 350 mW. An autocorrelation curve of the mode-locked pulses measured with a non-collinear second-harmonic autocorrelator is presented in Fig. 2. The curve exhibits a full-width-at-half-maximum (FWHM) of 20 ps, which corresponds to duration of 14 ps with a  $\text{sech}^2$  pulse profile.

We observed that the highest stable mode locking output from our laser depends on intracavity intensity. This is contradictory to what is expected from NLM effect. Note that at sufficiently high intracavity power, the spatial gain profile saturates and eventually loses the gain gradient needed for a stable mode locking with CSON. For Nd:YVO<sub>4</sub>, which is known to have a relative low saturation intensity, the saturation effect could be significant. We found that the intracavity intensity for the onset of mode-locking instability is about  $1.1 \times 10^3 \text{ W/cm}^2$ . The intensity is fairly close to the saturation intensity of Nd:YVO<sub>4</sub> ( $I_s \approx 1.3 \times 10^3 \text{ W/cm}^2$ ) [15]. When the output coupler was replaced with another one that has 20% transmission at the fundamental wave and high reflection at 532 nm, mode locking starts at 1.2 W at 808 nm. The mode locking becomes unstable when its output power is higher than 200 mW. Again the corresponding intracavity intensity is close to the saturation intensity of Nd:YVO<sub>4</sub>. The results of the laser output are presented in Fig. 3. To achieve stable mode-locking output from a gain medium that has low saturation intensity, the output coupler and spot sizes should be carefully compromised to minimize the gain saturation but maintain a high mode-locking strength.

Using first-order perturbation theory developed by Magni and co-workers [12,16], an analytical expres-

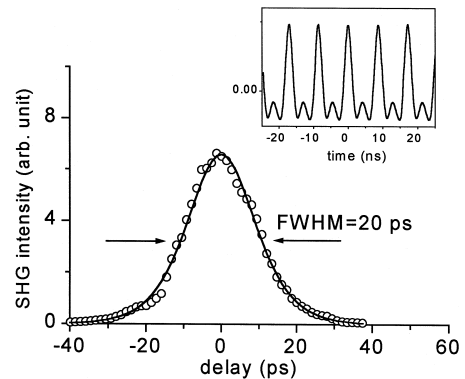


Fig. 2. Experimental noncollinear second-harmonic autocorrelation curve (symbols) of the mode-locked pulses. The pulse duration was determined to be 14 ps from a fit to a theoretical curve (solid line) using a  $\text{sech}^2$  pulse profile. The inset figure shows the CW mode-locked pulse train recorded with a digital oscilloscope.

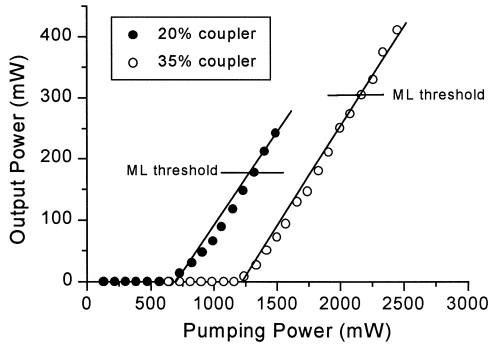


Fig. 3. Optical output at 1.064  $\mu\text{m}$  as a function of pumping power for two different output couplers.

sion for the nonlinear transmission variation in a resonator with NLM and CSON effects can be derived

$$\begin{aligned} \left(\frac{\delta T}{T}\right)_0 &= \frac{kL}{\pi} \gamma^2 P_F \\ &\times \left\{ -\text{Re} \left[ \int_{-L/2}^{L/2} S_F(z) \frac{\exp(-j\Delta kz)}{Q_F(z)} dz \right. \right. \\ &+ R_1 \left[ \int_{-L/2}^{L/2} S_B(z) \frac{\exp(j\Delta kz)}{Q_B(z)} dz \right. \\ &+ \left. \left. \left[ R_2 \frac{\text{Im}[q_F(L/2)]}{\text{Im}[q_B(L/2)]} \right]^{1/2} \left| S_F(L/2) \right. \right. \\ &\times \left. \left. \left[ \int_{-L/2}^{L/2} \frac{\exp(j\Delta kz)}{Q_B(z)} dz \right] \right] \right\}, \quad (4) \end{aligned}$$

where  $L$  denotes the nonlinear crystal length with its center position at  $z = 0$ ,  $R_1$  and  $R_2$  are the reflectivity of the fundamental and the second-harmonic waves at the output coupler, and  $S_F(z)$ ,  $S_B(z)$ ,  $Q_F(z)$  and  $Q_B(z)$  are defined as

$$S_F(z) = \int_{-L/2}^z \frac{\exp(j\Delta kz')}{q_F(z')} dz', \quad (5)$$

$$S_B(z) = \int_z^{L/2} \frac{\exp(-j\Delta kz')}{q_B(z')} dz', \quad (6)$$

$$Q_F(z) = \frac{L}{\text{Im}(q_F)} \left[ q_F^* - \frac{q_F^* + q_B}{2(q_F + q_B)} q_F \right], \quad (7)$$

$$Q_B(z) = \frac{L}{\text{Im}(q_B)} \left[ q_B^* - \frac{q_B^* + q_F}{2(q_B + q_F)} q_B \right]. \quad (8)$$

The  $q$ -parameters of the forward and backward propagating wave,  $q_F(z)$  and  $q_B(z)$ , can be calculated from the ABCD law  $q' = (Aq + B)/(Cq + D) = q$  with  $q$  and  $q'$  denoting the complex radius of curvature of the input and output beams, and  $A$ ,  $B$ ,  $C$ , and  $D$  the matrix elements of the round-trip transformation matrix. After solving the equation, the spot size can be deduced from the imaginary part of  $1/q$ . By transforming the  $q$  parameter with the ABCD law, the spot size at any position in cavity can be determined (see Fig. 4).

To reliably initiate and sustain a mode-locking output with a nonlinear loss modulation, the nonlinear transmission variation described by Eq. (4) must be positive and has magnitude as large as possible. For a laser without any intracavity aperture, we have  $q_F(z) = -q_B^*(z)$  and  $(\delta T/T)_0 = 0$  when  $R_1 = R_2$ . As pointed out by Magni and Zavelani-Rossi [16], the effects of intracavity apertures can be implicitly included into the round-trip self-consistent  $q$ -parameter. The gain profile originating from the pump beam can create an aperture effect. Assuming that the gain profile is identical to the pump profile, the amplified field  $E_0$  can then be related to an input

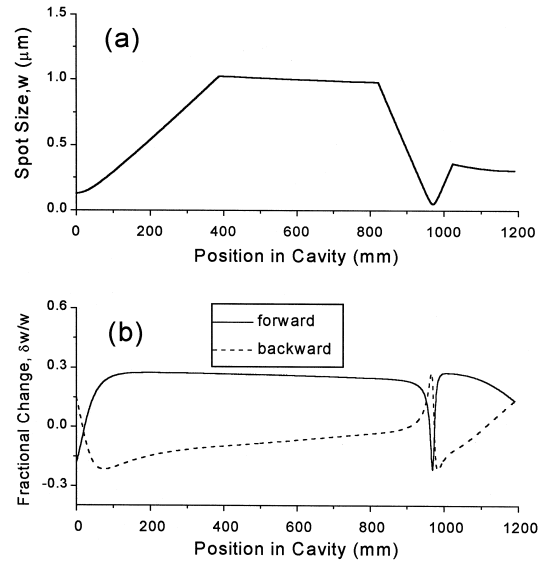


Fig. 4. (a) Spot size variation in the laser cavity; and (b) fractional change in spot size including the gain aperture effect.

field  $E_i$  at the pumping surface of the gain medium by

$$E_0(r) = G_0 \exp(-r^2/w_p^2) E_{i0} \exp(-r^2/w_o^2), \quad (9)$$

with  $G_0$  denoting the gain and  $w_p$  the pump waist. We can then take the gain-aperture effect into account by a transformation of  $1/q_0 = 1/q_i - j\lambda/\pi w_p^2$  at the pumping side. The pump waist of our laser was measured to be  $w_H = 140 \mu\text{m}$  in the sagittal plane and  $w_V = 165 \mu\text{m}$  in the tangential plane. Geometric average  $w_p = \sqrt{w_H w_V}$  was used to yield an effective spot size of the pump beam.

Fig. 5(a) shows the cavity spot size without the gain aperture effect. A fractional change of the spot size from the gain aperture in the forward- and backward-propagating direction was shown in Fig. 5(b). The laser cavity in Fig. 1 is stable when L2 is positioned between 102.1 cm and 104.8 cm relative to the pump surface of the gain medium. The mode locking was found to occur with L2 near the short-distance limit ( $\sim 102.1$  cm). This finding agrees with the prediction from Eq. (4), which shows that nonlinear transmission variation has a larger peak value (see Fig. 6) when L2 is close to the short-distance limit of the stability range. The nonlinear transmission variations shown in Fig. 6 have been normalized to that at the maximal conversion efficiency (i.e.,  $\eta_{\text{max}} = 2.1354(k/2\pi)\gamma^2 P_F$ ) [16]. We should also point out that the use of a lens (i.e., L2) instead of a mirror in Fig. 1 eliminates the need for cavity folding, and therefore avoids further astigma-

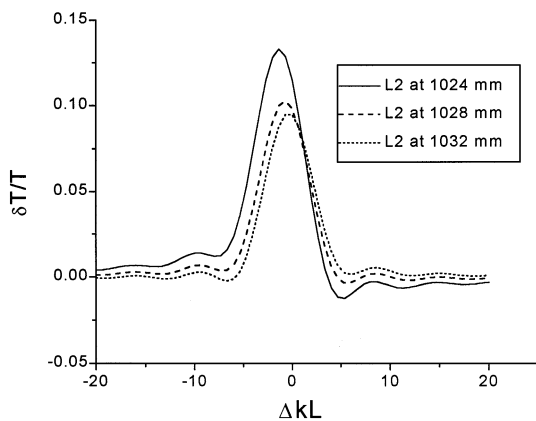


Fig. 5. Normalized nonlinear transmission variation as a function of phase mismatch at three different L2 positions.

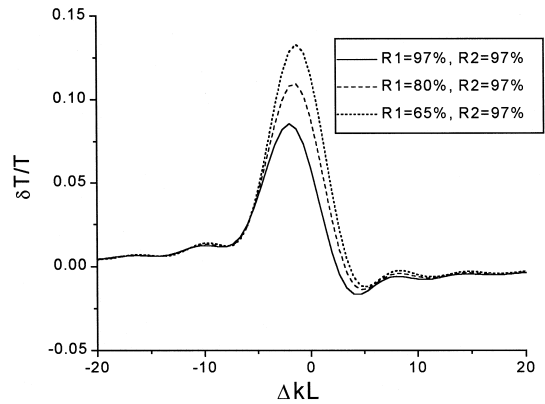


Fig. 6. Normalized nonlinear transmission variation as a function of phase mismatch for three different output couplers.

tism. Without astigmatism, both sagittal and tangential rays can be simultaneously brought as close as possible to the short-distance limit of the stability range to give larger mode-locking strength.

To compare the relative mode-locking strengths from the NLM and CSON effects, we present in Fig. 6 the curves of nonlinear transmission variation with different output couplers. In the calculations a 3% passive loss originating from incomplete back-conversion was taken into account by choosing  $R_2 = 97\%$ . The mode-locking strength from NLM was deduced from a comparison to the curve of nonlinear transmission variation with  $R_1 = R_2 = 97\%$ . From the calculated results, we found that in the case of  $R_1 = 65\%$  NLM contributes about 36% of the overall nonlinear transmission variation. With  $R_1 = 80\%$ , the contribution from NLM decreases to 22%. In both cases, CSON plays a major role in mode-locking the laser. However, when the gain saturation occurs, the mode-locking strength from CSON is weakened greatly. This leads to the on-set of the observed mode-locking instability. The mode locking process described here is different from another possible mode locking mechanism based on a combination of nonlinear rotation and an intracavity polarization-selecting element [17,18]. The fundamental field in our laser cavity has equal extraordinary and ordinary components in the type-II KTP crystal. The arrangement can not generate any nonlinear rotation.

The mode-locked laser can serve as a valuable source for characterizing nonlinear optical materials

with second harmonic microscopy [19–24]. A typical arrangement for the second-harmonic microscopy is depicted in Fig. 7. The generated second harmonic signal at 532 nm was filtered from the fundamental with a series of high quality short-pass and band-pass filters. The two-dimensional second harmonic intensity distribution is projected to a backside illuminated CCD camera via a microscopic objective ( $\times 10$ ) and a projection lens ( $\times 2.5$ ). The CCD has quantum efficiency more than 80% from 500 nm to 800 nm.

A periodically poled LiNbO<sub>3</sub> (PPLN) was selected for our second harmonic microscopic study. The surface of the PPLN had been etched with acids to convert the periodic domains into a surface profile. The resulting second harmonic image is shown in Fig. 8. It can be seen that the inverted domains generate stronger second-harmonic intensities than those from non-inverted regions (see Fig. 9(a)). The intensity variations in the second harmonic image is attributed to from the etching-induced thickness differences in ferroelectric domains

$$I_{2\omega} = \frac{2\sqrt{\epsilon_0 \mu_0^3} \omega^2 d^2}{n_\omega^2 n_{2\omega}} (I_\omega)^2 \frac{\sin^2\left(\frac{\pi L(x)}{2l_c}\right)}{\left(\frac{\pi}{2l_c}\right)^2}, \quad (10)$$

where  $I_\omega$  denotes the irradiance of the fundamental beam, the parameters,  $L(x)$  represents the thickness of the ferroelectric domains,  $n_\omega$  and  $n_{2\omega}$  are the refractive indices of LiNbO<sub>3</sub> at the fundamental and

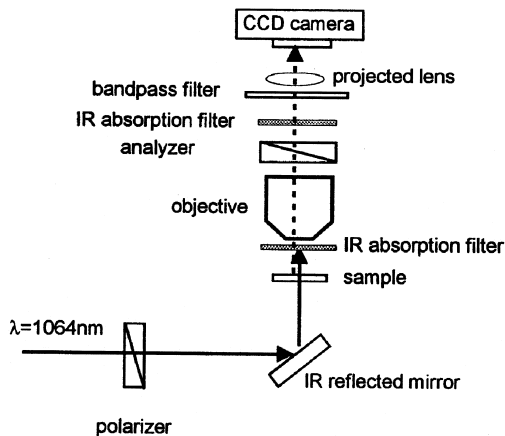


Fig. 7. Schematic of the second harmonic microscope.

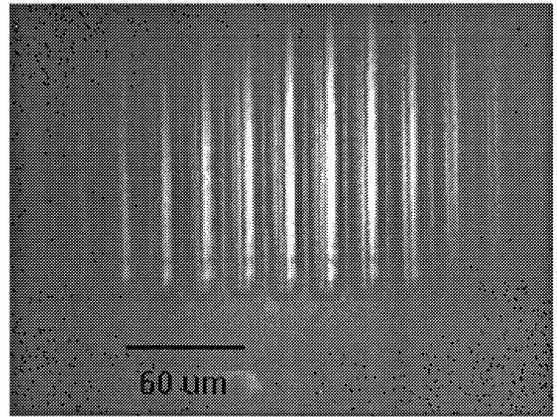


Fig. 8. Second harmonic image of a periodically poled LiNbO<sub>3</sub> (PPLN) substrate.

the second harmonic frequencies, and  $l_c = \pi/\Delta k$  depicts the coherent length. The etching profile of the ferroelectric domains can be deduced from the second-harmonic intensity distribution. The result is presented in Fig. 9(b). It merits to pointing out that the technique should also be applicable to investigate domain walls, which are embedded in the bulk of a ferroelectric crystal. However, the applications are out of the scope of this paper.

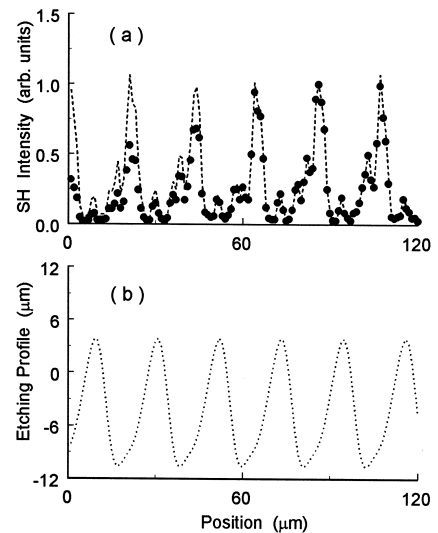


Fig. 9. (a) SH intensity profile (filled symbols) taken from Fig. 8, and corrected SH profile (dashed line) for the Gaussian distribution of the fundamental beam; and (b) the etching profile on the PPLN surface determined from the SH intensity profile shown in Fig. 9(a).

In summary, an inexpensive diode-pumped mode-locked Nd:YVO<sub>4</sub> laser had been constructed. Experimental observations agree well with the prediction from Magni's first-order perturbation theory. A self-defocusing effect from cascaded second-order optical nonlinearities (CSON) in a KTP crystal was found to dominate the observed mode locking process. The resulting self-defocusing lens couples with an effective aperture appearing in the gain medium to produce nonlinear loss modulation. The mode-locked laser is useful for second harmonic microscopy.

### Acknowledgements

We acknowledge the financial support from the National Science Council of the Republic of China under grant NSC 88-2112-M-009-039.

### References

- [1] D.E. Spence, P.N. Kean, W. Sibbett, *Opt. Lett.* 16 (1991) 42.
- [2] D.E. Spence, W. Sibbett, *J. Opt. Soc. Am. B* 8 (1991) 2053.
- [3] U. Keller, K.J. Weingarten, F.X. Kartner, D. Kopf, B. Braun, I.D. Jung, R. Fluck, C. Honninger, N. Matuschek, J. Aus der Au, *IEEE J. Sel. Topics Quantum Electron.* 2 (1996) 435.
- [4] L.R. Brovelli, U. Keller, T.H. Chiu, *J. Opt. Soc. Am. B* 12 (1995) 311.
- [5] K.A. Stankov, *Appl. Phys. B* 45 (1988) 191.
- [6] G. Cerullo, M.B. Danailov, S. De Silvestri, P. Laporta, V. Magni, D. Segala, S. Taccheo, *Appl. Phys. Lett.* 65 (1994) 2923.
- [7] A. Agnesi, C. Pennacchio, G.C. Reali, V. Kubecek, *Opt. Lett.* 22 (1997) 1645.
- [8] D. Pierrottet, B. Berman, M. Vannini, D. McGraw, *Opt. Lett.* 18 (1993) 263.
- [9] R. DeSalvo, D.J. Hagan, M. Sheik-Bahae, G. Stegeman, E.W. Van Stryland, H. Vanherzeele, *Opt. Lett.* 17 (1992) 28.
- [10] G. Cerullo, S. De Silvestri, A. Monguzzi, D. Segala, V. Magni, *Opt. Lett.* 20 (1995) 746.
- [11] G. Cerullo, V. Magni, A. Monguzzi, *Opt. Lett.* 20 (1995) 1785.
- [12] M. Zavelani-Rossi, G. Cerullo, V. Magni, *IEEE J. Quantum Electron.* 34 (1998) 61.
- [13] V. Magni, M. Zavelani-Rossi, *Opt. Commun.* 152 (1998) 45.
- [14] G.D. Boyd, *Nonlinear Optics*, Academic Press, San Diego, 1992 (Chapter 2).
- [15] L. DeShazer, *Laser Focus World* 30 (1994) 88.
- [16] V. Magni, M. Zavelani-Rossi, *J. Opt. Soc. Am.* 15 (1998) 2929.
- [17] V. Couderc, F. Louradour, A. Barthélémy, *Opt. Commun.* 166 (1999) 103.
- [18] V. Couderc, O. Guy, E. Roissé, A. Barthélémy, *Electron. Lett.* 34 (1998) 672.
- [19] K.A. Schultz, E.G. Seebauer, *J. Chem. Phys.* 97 (1992) 6958.
- [20] M. Flörsheimer, H. Salmen, M. Bösch, C. Brillert, M. Wierschem, H. Fuchs, *Adv. Mater.* 9 (1997) 1056.
- [21] M. Flörsheimer, H. Salmen, M. Bösch, C. Brillert, M. Wierschem, H. Fuchs, *Adv. Mater.* 9 (1997) 1061.
- [22] S. Kurimura, Y. Uesu, *J. Appl. Phys.* 81 (1997) 369.
- [23] L. Smilowitz, Q.X. Jia, X. Yang, D.Q. Li, D. McBranch, S.J. Buelow, J.M. Robinson, *J. Appl. Phys.* 81 (1997) 2051.
- [24] M. Cernusca, M. Hofer, G.A. Reider, *J. Opt. Soc. Am. B* 15 (1998) 2476.